Available online at www.sciencedirect.com
ScienceDirect
International Journal of Heat and Mass Transfer 50 (2007) 2859–2873
International Journal of HEAT and MASS TRANSFER
www.elsevier.com/locate/ijhmt

Topology optimization of convection-dominated, steady-state heat transfer problems

T.E. Bruns

Beckman Institute for Advanced Science and Technology, University of Illinois at Urbana-Champaign, Urbana, IL 61801, USA

Received 2 November 2006; received in revised form 24 January 2007
Available online 29 March 2007

Abstract

The current push in the topology optimization community is to apply topology optimization to mechanics problems beyond typical structural design to other physical domains. Here, a framework for topology optimization of nonlinear steady-state heat transfer with conduction, convection, and radiation without explicitly accounting for fluid motion is evaluated. Convection-dominated diffusion problems are susceptible to numerical instabilities that, unless they are handled properly in the analysis, can severely affect the optimization. This numerical instability issue is the focus of this work, its origin is discussed in the context of density-design-variable-based topology optimization, and a method for avoiding such instabilities is described. Several design examples demonstrate the approach.

Keywords: Topology optimization; Heat transfer; Conduction; Convection

1. Introduction

Until recently, topology optimization has been primarily applied to structural problems. We apply topology optimization to steady-state heat transfer problems here. The methodology of structural topology optimization can be applied to conduction heat transfer problems in a relatively straightforward manner. For example, Fig. 1a depicts the design domain of an insulated enclosure that is subject to volumetric heat generation and a heat sink at the mid-span of the left domain edge. The goal is optimally place a limited amount of conductive material within the design domain so that the maximum temperature is minimized in a manner analogous to minimum compliance for structural topology optimization problems. The notion of topology is introduced by weighting the conduction matrix by a design-variable-dependent density measure, i.e. in the same manner as the stiffness matrix is typically weighted for structural problems. The optimal distribution of highly conductive material as depicted in Fig. 1b is reminiscent of tree-like structures found in nature. We can imagine that a micro-cooler for a tightly packed VLSI electronic system could be based on the distribution of the conduction channels depicted in Fig. 1b. Because the governing equation, i.e. Poisson equation, associated with heat transfer defines other field problems, e.g. electric and magnetic potential, ideal fluid flow, etc., the same methodology can be applied to many diverse physical problems.

Extensive work has previously addressed the design sensitivity computation for thermal-based shape optimization problems, e.g. refer to the comprehensive summary in [1], so we briefly examine the research literature that accounts for thermal effects and similar field problems specifically using topology optimization techniques. A similar formulation of the field problem of Fig. 1 appears in the work by Borrvall et al. [2], i.e. in the context of porous media flow, and Bendsøe and Sigmund [3], i.e. in the context of conduction heat transfer. Rodrigues and Fernandes [4,5] and Jog [6] investigated thermoelasticity early in the history of topology optimization. Li et al. [7–10,1] have extensively applied evolutionary structural optimization to thermoelastic and heat transfer topology design problems, and they apply evolutionary structural optimization to general

E-mail address: tbruns@uiuc.edu

0017-9310/$ - see front matter © 2007 Elsevier Ltd. All rights reserved.
doi:10.1016/j.ijheatmasstransfer.2007.01.039

Nomenclature

a	area
A	cross-sectional area
c_p	specific heat
d_i	ith design variable
$\underline{d}_i$, $\bar{d}_i$	lower and upper bounds
$\mathbf{d}$	design variable field
g	side convection function
h	convection coefficient
$\bar{h}$	nominal convection coefficient
k	thermal conductivity
$\mathbf{K}$	thermal conductance matrix
$\mathbf{K}_T$	tangent matrix
L	length
$\mathbf{n}$	outward normal
nc	number of optimization constraints
nd	number of design variables
$\mathbf{N}$	shape function matrix
p	penalty parameter
P	perimeter
$\mathbf{P}$	thermal load vector
$\mathbf{q}$	heat flux vector
$q^{\mathbf{n}}$	surface heat flux
q^*	prescribed surface heat flux
q_b^*	prescribed surface heat flux at the base
Q	heat generation rate per unit volume
$\mathbf{R}$	residual
s	heat source
s_{ij}	distance from centroid of element j to element i
T	excess temperature field
T_b^*	prescribed excess temperature at the base
v	volume
$\bar{v}$	upper volume bound
$\mathbf{v}$	fluid velocity vector
x, $\mathbf{x}$	material point location in one- and multi-dimensions

Greek symbols

α	penalty parameter
$\epsilon_{\mathbf{R}}$, $\epsilon_{\mathbf{\Theta}}$	convergence tolerances
η_1, $\hat{\eta}_1$	first density measure value and function
$\boldsymbol{\eta}_1$	first density measure field
η_2, $\hat{\eta}_2$	second density measure value and function
$\boldsymbol{\eta}_2$	second density measure field
Γ	surface
Γ_q, Γ_θ	complementary subsurfaces
ω_i	sum of filter kernel weights
$\omega_j(s_{ij})$	filter kernel
Ω	interior
ϕ, $\hat{\phi}$	filtered density design variable and function
$\boldsymbol{\phi}$	filtered density design variable field
ρ	fluid density
θ	temperature field
θ^*	prescribed temperature field
$\mathbf{\Theta}$	nodal temperature field
$\mathbf{\Delta\Theta}$	temperature update
Θ_0, Θ_i	optimization objective and constraints

Superscripts

h	convective (and radiative) contribution
k	conductive contribution
q	imposed surface heat flux contribution
Q	concentrated heat source contribution

physical field problems [11]. Kikuchi and coworkers early examined piezoelectric material and mechanism topology design, e.g. in [12,13] and implemented transient heat conduction for topology design [14]. In a manner similar to the methods developed for structural topology optimization, topology optimization has been applied to electromagnetic design problems, e.g. in [15–17]. Sigmund and coworkers first investigated the thermal effects on material layout design [18–20] and first introduced heat transfer and electrical conduction into the inherently multiphysical topology design problem for microelectromechanical (MEM) systems [21–23]. Yin and Ananthasuresh [24] and Yoon and Kim [25] have subsequently investigated similar MEM design problems. Maute and coworkers [26,27] investigate electrostatically actuated MEM systems. Bruns and Sigmund [28] investigated the topology design of mechanisms that exhibit snap-through due to thermally-induced strain. More recently, Ha et al. [29] and Moon et al. [30] investigate nonlinear heat conduction and heat transfer with convection topology design problems, respectively, along the lines investigated here.

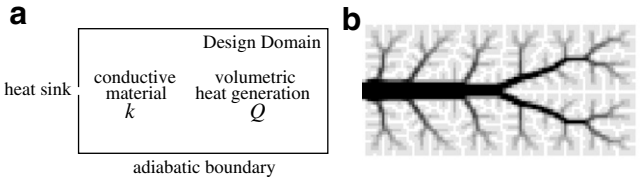

Fig. 1. (a) Design domain of an adiabatic enclosure with volumetric heat generation and heat sink. (b) Optimal distribution of highly conductive material.

Here, we investigate convection-dominated heat transfer topology design problems and the numerical instabilities that develop due to low density elements in the finite element analysis (FEA) of the topology optimization. We illustrate the potential problems by examining the FEA of the cooling fin embedded in the fixed $8 \times 8\ \text{mm}^2$ mesh discretized by 64 4-noded quadrilateral elements and depicted in Fig. 2. The black elements of the cooling fin

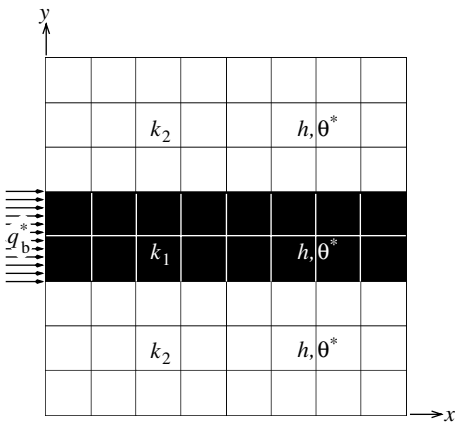

Fig. 2. Cooling fin embedded in fixed domain.

has high thermal conductivity k_1 and the cooling fin is embedded in a fluid denoted by white elements with relatively low thermal conductivity $k_2 \ll k_1$. We apply a uniform heat flux along the left edges of the two leftmost elements of the cooling fin and also apply convection with coefficient h and ambient fluid temperature $\theta^* = 0$ °C uniformly over the planar surface of the entire domain. Fig. 3a shows the temperature contour plot of the cooling fin examined by FEA using the usual consistent discretization of the governing nonlinear heat transfer equations with convection. Note that the temperature denoted in the black regions falls below the ambient fluid temperature θ^*. The nonphysical oscillations are apparent in the temperature profiles plotted at discrete intervals along the cooling fin length of Fig. 3b. These oscillations are due to the introduction of convection into the heat transfer problem and large orders of magnitude difference between the thermal conductivities in the FEA. Such "wiggles" are an emphatic sign that the finite element methodology cannot correctly capture the underlying physics [31]. Note that such conditions will invariably occur in the topology optimization of heat transfer problems with convection because of the density-design-variable-weighted thermal conductivities. Moreover, we cannot accept the poor performance of the FEA because this spurious behavior can adversely

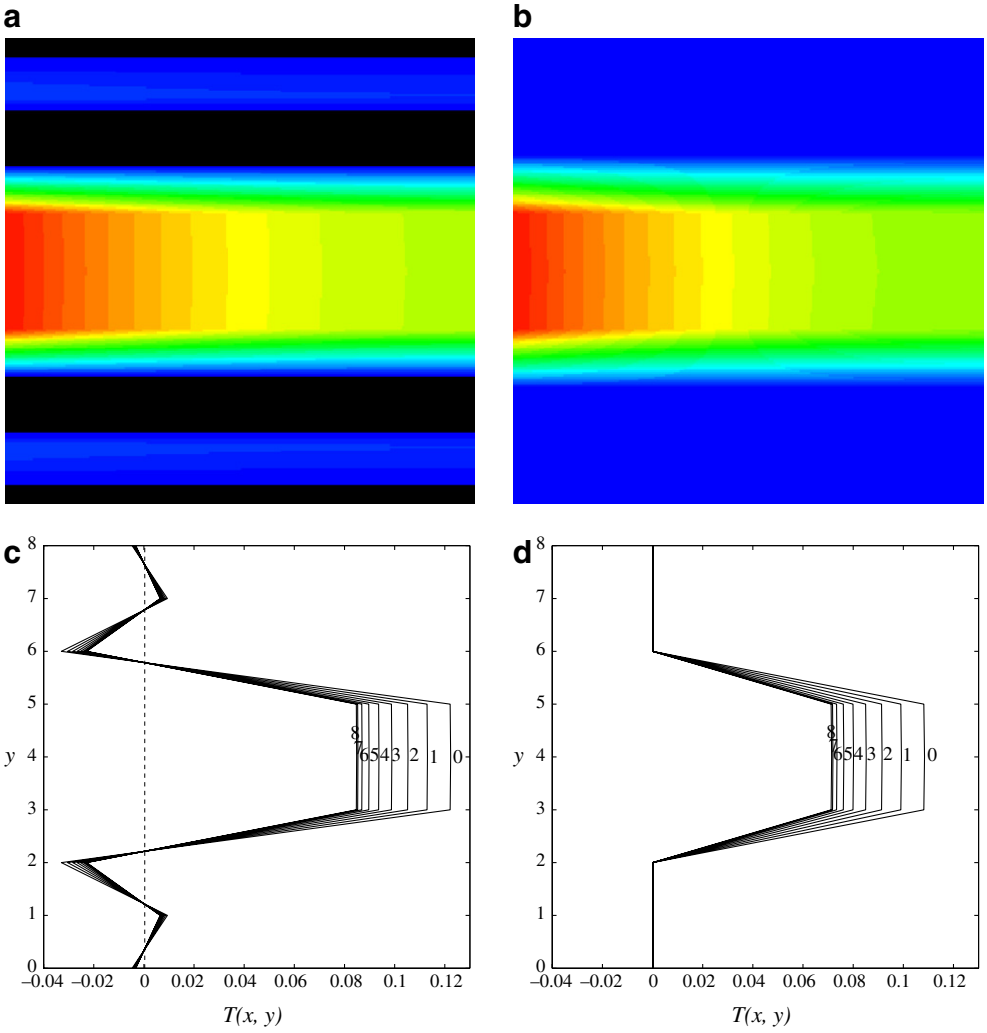

Fig. 3. Temperature contour plots of cooling fin by FEA using (a) consistent and (b) lumped convection matrices. Corresponding temperature response profile plots at (0) $x = 0$, (1) 1, (2) 2, (3) 3, (4) 4, (5) 5, (6) 6, (7) 7, and (8) 8 mm for (c) consistent and (d) lumped convection matrices.

affect the topology optimization iterative design space search. Yoon and Kim [25] highlight this problem for multiphysics problems, and they conclude that there is no density-based interpolation scheme that can resolve the numerical instabilities, and therefore they justify a new topology optimization approach, the element connectivity parameterization (ECP) method, that circumvents the problem. We also encountered the oscillatory behavior in the topology optimization of MEM devices [32]. However, we resolve the numerical instability problem directly as Fig. 3b and d suggest.

In Section 2, we develop the governing heat transfer equations. Topology optimization is briefly defined in Section 3. Then, we closely examine why the oscillatory behavior develops in the heat transfer analysis by comparing analytical and finite element analyses, and we propose a remedy in Section 4. In Section 5, we illustrate our approach by generating several topology designs by example.

2. Heat transfer analysis

The arbitrary body of Fig. 4 distinguished by its interior Ω and surface Γ is subjected to heat transfer. The global steady-state heat transfer equilibrium equation that balances the net surface heat flux $q^{\mathbf{n}}$ over Γ denoted by outward orientation normal $\mathbf{n}$ exiting the system with the net heat source s added to Ω is expressed for each material point $\mathbf{x}$ as

$$-\int_{\Gamma} q^{\mathbf{n}}(\mathbf{x})\,\mathrm{d}a + \int_{\Omega} s(\mathbf{x})\,\mathrm{d}v = 0 \tag{1}$$

and solved for the temperature distribution $\theta(\mathbf{x})$. We differentiate between complementary subsurfaces where the temperature field is prescribed, i.e. on Γ_θ, and the surface heat flux is applied or adiabatic conditions assumed, i.e. on Γ_q, such that $\Gamma_\theta \cup \Gamma_q \equiv \Gamma$ and $\Gamma_\theta \cap \Gamma_q = 0$. From Cauchy's theorem, the heat flux vector $\mathbf{q}$ is defined through

$$q^{\mathbf{n}}(\mathbf{x}) \equiv \mathbf{q}(\mathbf{x}) \cdot \mathbf{n}(\mathbf{x}) \tag{2}$$

and, using the divergence theorem, leads to the local energy balance for $\mathbf{x} \in \Omega$ expressed as

$$-\mathrm{div}\,\mathbf{q}(\mathbf{x}) + s(\mathbf{x}) = 0. \tag{3}$$

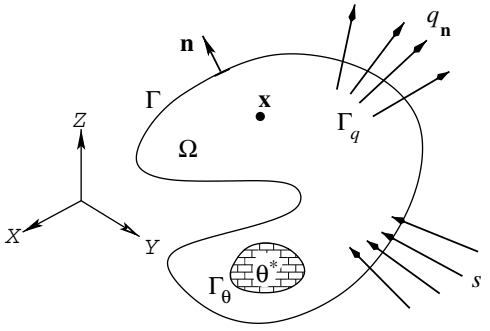

Fig. 4. Body subjected to heat transfer.

We assume that the constitutive material obeys Fourier's law, i.e.

$$\mathbf{q}(\mathbf{x}) = -k(\theta(\mathbf{x}), \mathbf{x})\nabla\theta(\mathbf{x}) \tag{4}$$

where the isotropic thermal conductivity k is potentially temperature dependent. In addition to prescribed temperature field θ^* on $\mathbf{x} \in \Gamma_\theta$

$$\theta(\mathbf{x}) = \theta^*(\mathbf{x}), \tag{5}$$

surface heat flux or convective boundary conditions are prescribed for $\mathbf{x} \in \Gamma_q$ by

$$q^{\mathbf{n}}(\mathbf{x}) = q^*(\mathbf{x}) \quad \text{or} \tag{6}$$

$$q^{\mathbf{n}}(\mathbf{x}) = h(\theta(\mathbf{x}), \theta^*(\mathbf{x}), \mathbf{x})(\theta(\mathbf{x}) - \theta^*(\mathbf{x})), \tag{7}$$

respectively, note that radiation boundary conditions can be readily recast mathematically in the form of a nonlinear convective boundary condition.

Upon discretization of the domain by a finite element mesh, the governing equations to solve for the nodal temperature field $\boldsymbol{\Theta}$ are expressed algebraically in residual $\mathbf{R}$ form as

$$\mathbf{R}(\boldsymbol{\Theta}) = -\mathbf{K}(\boldsymbol{\Theta})\boldsymbol{\Theta} + \mathbf{P}(\boldsymbol{\Theta}) \tag{8}$$

where the thermal conductance matrix $\mathbf{K}$ and thermal load vector $\mathbf{P}$ are further decomposed by

$$\mathbf{K} = \mathbf{K}^k + \mathbf{K}^h \quad \text{and} \tag{9}$$

$$\mathbf{P} = \mathbf{P}^Q + \mathbf{P}^q + \mathbf{P}^h \tag{10}$$

where superscripts k, h, Q, and q denote conductive, convective (and radiative), concentrated heat source, and imposed surface heat flux contributions, respectively, Refer to references such as [33] for a more thorough numerical treatment of these terms. Since $\mathbf{K}$ and $\mathbf{P}$ are generally nonlinear with respect to $\boldsymbol{\Theta}$, we use the Newton–Raphson method to iteratively compute the temperature update $\Delta\boldsymbol{\Theta}$ at iteration i by

$$\mathbf{K}_{\mathrm{T}}(\boldsymbol{\Theta}_i)\Delta\boldsymbol{\Theta} = \mathbf{R} \tag{11}$$

$$\boldsymbol{\Theta}_{i+1} = \boldsymbol{\Theta}_i + \Delta\boldsymbol{\Theta} \tag{12}$$

with tangent matrix $\mathbf{K}_{\mathrm{T}} \equiv -\frac{\partial \mathbf{R}}{\partial \boldsymbol{\Theta}}$ until convergence is satisfied, e.g. by

$$\|\mathbf{R}_i\| \leqslant \epsilon_{\mathbf{R}} \quad \text{and} \quad \|\Delta\boldsymbol{\Theta}\| \leqslant \epsilon_{\boldsymbol{\Theta}} \tag{13}$$

for $\epsilon_{\mathbf{R}} \ll 1$ and $\epsilon_{\boldsymbol{\Theta}} \ll 1$.

3. Topology optimization

The topology optimization problem is stated as

$$\text{minimize} \quad \Theta_0(\mathbf{d}) \tag{14}$$

$$\text{subject to} \quad \Theta_i(\mathbf{d}) \leqslant 0 \tag{15}$$

$$\underline{d}_j \leqslant d_j \leqslant \overline{d}_j \tag{16}$$

where Θ_0 is the objective function, $\Theta_i (\text{for } i = 1, nc)$ are the inequality constraints and $d_j (\text{for } j = 1, nd)$ are the design variables that are bounded above and below by $\overline{d}_j$ and $\underline{d}_j$.

Although the density design variables can be assigned to nodes, and then the field is appropriately interpolated, a density design variable d_i is assigned to every element i here that ranges between its small lower bound $\underline{d}_i \approx 0$, e.g. $\underline{d}_i = 10^{-6}$, and upper bound $\overline{d}_i = 1$. The notion of topology is introduced into the analysis through a set of first density measures η_1 which indicates the presence or absence of the influence of a physical property, e.g. by

$$\mathbf{K}_i^k = \hat{\eta}_{1i}^k(\mathbf{d})\widehat{\mathbf{K}}_i^k \tag{17}$$

for conduction heat transfer and

$$\mathbf{K}_i^h = \hat{\eta}_{1i}^h(\mathbf{d})\widehat{\mathbf{K}}_i^h \tag{18}$$

$$\mathbf{P}_i^h = \hat{\eta}_{1i}^h(\mathbf{d})\widehat{\mathbf{P}}_i^h \tag{19}$$

for convection (and radiation) heat transfer where the $\widehat{\mathbf{K}}$ and $\widehat{\mathbf{P}}$ right-hand-side terms correspond to the full presence of the physical property and the $\mathbf{K}$ and $\mathbf{P}$ left-hand-side terms are used in the computational analysis. Note that the first density measure η_{1i} is computed for every finite element i and is defined as a function of the density design variable field $\mathbf{d}$, i.e. $\eta_{1i} = \hat{\eta}_{1i}(\mathbf{d})$. In a manner consistent with the density design variable range, the density measure η_1 ranges from a small value to one representing the absence or presence of the property, respectively. Since we are interested in the topology of the material in Ω, the variation in the first density measure field $\boldsymbol{\eta}_1^k$ is used to depict the topology of the body subjected to heat transfer.

There are a variety of ways to introduce the notion of topology into the FEA of the topology optimization problem. The most common approach is by the SIMP method [34,35], but we apply the SINH ("cinch") method here which is more fully described in [36]. Briefly, the method penalizes less volumetrically effective intermediate density material, and compared to previous filter techniques, the "regularization" is moved from the primal analysis, through η_1, to the resource constraint, through η_2. We define both the SIMP and SINH methods independent of the particular interpolation function chosen, e.g. power law, hyperbolic sine, etc. Here, the linear first η_1^k and power law second η_2 density measures for every element i are defined by

$$\eta_{1i}^k = \hat{\eta}_{1i}^k(\mathbf{d}) = d_i \quad \text{and} \tag{20}$$

$$\eta_{2i} = \hat{\eta}_{2i}(\mathbf{d}) = 1 - (1 - \phi_i)^p \tag{21}$$

where the filtered density design variable field $\boldsymbol{\phi}$ is computed for every element i as

$$\phi_i = \hat{\phi}_i(\mathbf{d}) = \sum_j \frac{\omega_j(s_{ij})}{\omega_i} d_j \tag{22}$$

with

$$\omega_i = \sum_j \omega_j(s_{ij}) \tag{23}$$

and the Gaussian-weighted kernel ω_j computed by

$$\omega_j(s_{ij}) = \begin{cases} \dfrac{\exp\left(-\frac{s_{ij}^2}{2\left(\frac{r}{3}\right)^2}\right)}{2\pi\left(\frac{r}{3}\right)} & \text{for } s_{ij} \leqslant r \\ 0 & \text{for } s_{ij} > r \end{cases} \tag{24}$$

is based on the distance s_{ij}, e.g.

$$s_{ij} = ((x_j - x_i)^2 + (y_j - y_i)^2)^{\frac{1}{2}}, \tag{25}$$

of the surrounding element j centroids (x_j, y_j) within a fixed mesh-independent radius r of the element i centroid (x_i, y_i). The appropriate definition of the first density measure η_1^h due to the convection terms is the subject of the next section. We define the effective volume v, corresponding to the design domain Ω, as

$$v(\mathbf{d}) = \int_\Omega \hat{\eta}_2(\mathbf{d})\,\mathrm{d}v, \tag{26}$$

and we constrain v by its upper bound $\bar{v}$ defined as a fraction of the maximal volume $\int_\Omega \mathrm{d}v$, i.e.

$$\Theta_1(\mathbf{d}) = v(\mathbf{d}) - \bar{v}. \tag{27}$$

As the penalty parameter $p \geqslant 1$ is increased, the volume is progressively penalized, and therefore, the intermediate density material is volumetrically less effective. Since intermediate density material consumes more volume with respect to its load carrying capability than solid or void material, the topology optimization algorithm will redistribute, i.e. within the constraints of the mesh discretization, the intermediate density material of given volume more effectively.

Analytical sensitivities, i.e. $\frac{\mathrm{d}\Theta_0}{\mathrm{d}\mathbf{d}}(\mathbf{d})$ and $\frac{\mathrm{d}\Theta_i}{\mathrm{d}\mathbf{d}}(\mathbf{d})$, are calculated efficiently here by the adjoint method [37], and the Method of Moving Asymptotes (MMA) [38] is used to solve the large-scale optimization problem.

4. Numerical instabilities

We investigate numerical instabilities that can develop in convection-dominated diffusion problems due to the density dependent interpolation schemes of topology optimization. We emphasize here that we investigate the temperature response due to changes in the material properties, e.g. thermal conductivity k, which is tantamount to varying the design variables $\mathbf{d}$ of the density measures $\boldsymbol{\eta}_1$ that weight the corresponding material properties, e.g. the $\mathbf{d}$ of $\hat{\eta}_{1i}^k(\mathbf{d})$ in Eq. (17).

Consider the one-dimensional heat conduction problem of the fins depicted in Fig. 5 subject to conduction, convection, and possible heat generation. We arbitrarily decompose the fins into two domains to investigate the convergent behavior of the temperature response as the physical properties of the second domain Ω_2 vanish.

To determine the temperature $\theta(x)$ distribution in the x-direction, the governing equation for one-dimensional steady-state heat conduction subject to appropriate boundary conditions is expressed as

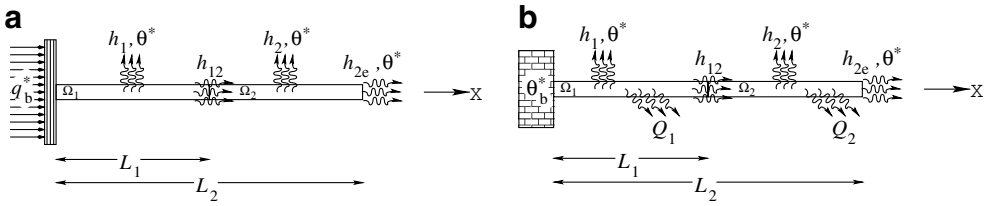

Fig. 5. Fins composed of domains Ω_1 and Ω_2 subjected to one-dimensional heat transfer (a) with prescribed base heat flux (problem P1) and (b) with heat generation and prescribed base temperature (problem P2).

$$\frac{\mathrm{d}}{\mathrm{d}x}\left(k(\theta(x),x)A(x)\frac{\mathrm{d}\theta(x)}{\mathrm{d}x}\right) - h(\theta(x),x)P(x)(\theta(x)-\theta^*) + Q(\theta(x),x)A(x) = 0 \tag{28}$$

where k is the thermal conductivity, A is the cross-sectional area, h is the convection heat transfer coefficient, P is the perimeter, θ^* is the ambient fluid temperature far removed from the body, and Q is the heat generation rate per unit volume. The excess temperature field $T(x)$ is defined by

$$T(x) \equiv \theta(x) - \theta^*. \tag{29}$$

Assuming k, h, and Q are independent of temperature and k, h, Q, A, and P are constant over the region of interest, then

$$\frac{\mathrm{d}^2T}{\mathrm{d}x^2} - m^2T = -\frac{Q}{k} \tag{30}$$

is subject to appropriate boundary conditions and

$$m^2 \equiv \frac{hP}{kA}. \tag{31}$$

Without loss of generality, we assume that the fin is of uniform, unit cross-sectional area and perimeter.

In Ω_1 for $0 \leqslant x \leqslant L_1$ of the fins, the corresponding excess temperature field T_1 is found by

$$\frac{\mathrm{d}^2T_1}{\mathrm{d}x^2} - m_1^2T_1 = -\frac{Q_1}{k_1} \tag{32}$$

for $m_1^2 = \frac{h_1}{k_1}$. For the fin of problem P1 in Fig. 5a, Eq. (32) is subject to the prescribed surface heat flux at the base q_b^* where

$$q_1^x(0) = -k_1\left.\frac{\mathrm{d}T_1}{\mathrm{d}x}\right|_{x=0} = q_\mathrm{b}^*, \tag{33}$$

and no heat generation, i.e. $Q_1 = 0$. For the fin of problem P2 in Fig. 5b, Eq. (32) is subject to

$$T_1(0) = T_\mathrm{b}^* = \theta_\mathrm{b}^* - \theta^* \tag{34}$$

where the excess temperature $T_1(0)$ at the base, i.e. $x = 0$, is prescribed as T_b^*. In Ω_2 for $L_1 \leqslant x \leqslant L_2$,

$$\frac{\mathrm{d}^2T_2}{\mathrm{d}x^2} - m_2^2T_2 = -\frac{Q_2}{k_2} \tag{35}$$

for $m_2^2 = \frac{h_2}{k_2}$ subject to

$$h_{2e}T_2(L_2) = -k_2\left.\frac{\mathrm{d}T_2}{\mathrm{d}x}\right|_{x=L_2} \tag{36}$$

where h_{2e} is the convection coefficient at $x = L_2$, and $Q_2 = 0$ for the fin of Fig. 5a. For continuity, we enforce

$$T_1(L_1) = T_2(L_1) \tag{37}$$

across the Ω_1–Ω_2 interface. In addition, to evaluate the behavior as Ω_2 vanishes, we define convection at the interface by

$$h_{12}T_1(L_1) = -k_1\left.\frac{\mathrm{d}T_1}{\mathrm{d}x}\right|_{x=L_1} + k_2\left.\frac{\mathrm{d}T_2}{\mathrm{d}x}\right|_{x=L_1} \tag{38}$$

where h_{12} is the convection coefficient at the interface $x = L_1$. Note that when $h_{12} \to 0$, $k_1\frac{\mathrm{d}T_1}{\mathrm{d}x}|_{x=L_1} = k_2\frac{\mathrm{d}T_2}{\mathrm{d}x}|_{x=L_1}$ for continuity, and when $k_2 \to 0$, then $h_{12}T_1(L_1) = -k_1\frac{\mathrm{d}T_1}{\mathrm{d}x}|_{x=L_1}$.

Next, we analytically evaluate the temperature response of the fins as the physical properties of the second domain Ω_2 vanish. For illustrative purposes, we assign values of one to parameters that exist and small values, e.g. 10^{-6}, to parameters that vanish. For Ω_1, we set $L_1 = 1$ m, $k_1 = 1\ \frac{\mathrm{W}}{\mathrm{m}\,^\circ\mathrm{C}}$, $h_1 = 1\ \frac{\mathrm{W}}{\mathrm{m}^2\,^\circ\mathrm{C}}$, and $Q_1 = 0$ W, and for Ω_2, we set $L_2 - L_1 = 1$ m and $Q_2 = 0$ W. For P1, we prescribe the heat flux $q_\mathrm{b}^* = 1\ \frac{\mathrm{W}}{\mathrm{m}^2}$ at the base and the ambient fluid temperature $\theta^* = 0\ ^\circ\mathrm{C}$. When Ω_2 exists, we set $k_2 = 1\ \frac{\mathrm{W}}{\mathrm{m}\,^\circ\mathrm{C}}$, $h_2 = h_1 = 1\ \frac{\mathrm{W}}{\mathrm{m}^2\,^\circ\mathrm{C}}$, $h_{12} = 0\ \frac{\mathrm{W}}{\mathrm{m}^2\,^\circ\mathrm{C}}$, and $h_{2e} = 1\ \frac{\mathrm{W}}{\mathrm{m}^2\,^\circ\mathrm{C}}$. The corresponding baseline temperature response is depicted in Fig. 6a.

We expect that the temperature should approach the ambient fluid temperature $\theta^* = 0\ ^\circ\mathrm{C}$ in Ω_2 as Ω_2 vanishes because there is no constituent material to conduct the

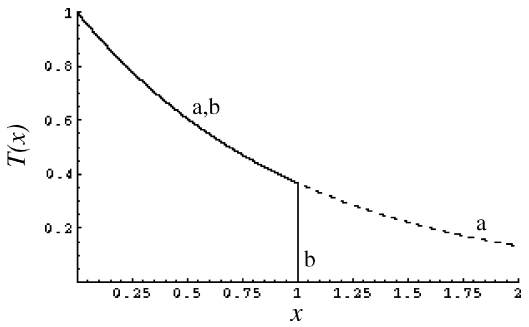

Fig. 6. (P1) Analytical excess temperature response $T(x)$ for (a) Ω_2 present and (b) absent/vanishing Ω_2.

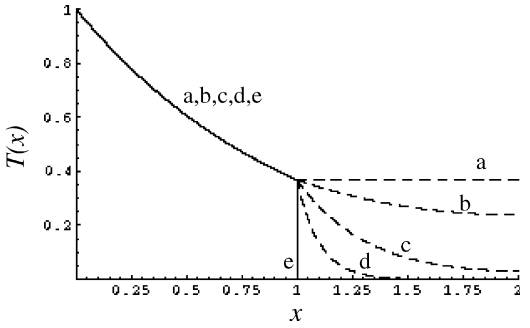

Fig. 7. (P1) Convergent behavior of the excess temperature $T(x)$ for (a) $h_2 = 10^{-9}$, (b) 10^{-6}, (c) 10^{-5}, (d) 10^{-4}, and (e) $1\ \frac{\mathrm{W}}{\mathrm{m}^2\,^\circ\mathrm{C}}$.

heat. For vanishing Ω_2, we set $k_2 = 10^{-6}\ \frac{\mathrm{W}}{\mathrm{m}\,^\circ\mathrm{C}}$, $h_{12} = 1\ \frac{\mathrm{W}}{\mathrm{m}^2\,^\circ\mathrm{C}}$, and $h_{2e} = 0\ \frac{\mathrm{W}}{\mathrm{m}^2\,^\circ\mathrm{C}}$, and we vary the convection coefficient h_2 to study the asymptotic behavior of the temperature response. Fig. 7 indicates that the value of h_2 should be independent of the presence or absence of Ω_2. Consequently, the correct temperature response with $h_2 = h_1 = 1\ \frac{\mathrm{W}}{\mathrm{m}^2\,^\circ\mathrm{C}}$ is depicted in Fig. 6b (and Fig. 7e).

Next, we examine the temperature response computed by conventional FEA. The volumetric conductive and convective contributions to $\mathbf{K}$ and $\mathbf{P}$ are

$$\mathbf{K}^k = \int_\Omega \nabla^{\mathrm{T}}\mathbf{N} k \nabla\mathbf{N}\,\mathrm{d}v, \quad \mathbf{K}^h = \int_\Omega \mathbf{N}^{\mathrm{T}} h \mathbf{N}\,\mathrm{d}v, \quad \text{and}$$
$$\mathbf{P}^h = \int_\Omega \mathbf{N}^{\mathrm{T}} h\theta^*\,\mathrm{d}v \tag{39}$$

for an isotropic material with conductivity coefficient k, where we assume that h is constant over each domain of influence and $\mathbf{N}$ is the shape function matrix consistent with the particular finite element discretization. For one-dimensional, two-noded elements with uniform, unit cross-sectional area, perimeter, and length, i.e. $A = P = L = 1$, the above terms are evaluated as

$$\mathbf{K}^k = k\begin{bmatrix} 1 & -1 \\ -1 & 1 \end{bmatrix}, \quad \mathbf{K}^h = \frac{h}{6}\begin{bmatrix} 2 & 1 \\ 1 & 2 \end{bmatrix}, \quad \text{and} \quad \mathbf{P}^h = \frac{h\theta^*}{2}\begin{Bmatrix} 1 \\ 1 \end{Bmatrix} \tag{40}$$

in a *consistent* manner.

We evaluate the temperature response of problem P1 for vanishing Ω_2. Fig. 8 shows the FEA response to P1 when $k_2 = 10^{-6}\frac{\mathrm{W}}{\mathrm{m}\,^\circ\mathrm{C}}$, $h_{12} = 1\ \frac{\mathrm{W}}{\mathrm{m}^2\,^\circ\mathrm{C}}$, and $h_{2e} = 0\ \frac{\mathrm{W}}{\mathrm{m}^2\,^\circ\mathrm{C}}$, and $h_2 = h_1 = 1\ \frac{\mathrm{W}}{\mathrm{m}^2\,^\circ\mathrm{C}}$. Note that there are oscillations in the temperature response which indicate that the finite element discretization does not accurately capture the physics of the problem. Although h- and p-refinement can reduce the magnitude of the oscillations, neither can resolve the numerical instability. From a practical point of view, if the analyst is merely interested in the heat transfer analysis, they might be satisfied with the temperature response in Ω_1 and accept that the temperature response in Ω_2 does not reflect the physics of the problem. However, since we are interested in design by topology optimization, we cannot model the physics incorrectly and expect that the optimization algorithm in general will ignore the poor modeling, and in many cases the optimizer will take advantage of the incorrect modeling.

Numerical oscillations are a well known phenomena in the computational response of convection-dominated fluid mechanics problems where adding artificial viscosity remedies the oscillations. Analogous to adding artificial viscosity, we could add artificial conductive material when oscillations appear in the analysis. However, it is not readily apparent how and when the artificial conductivity should be added so that the temperature response remains consistent and continuous between design changes of the optimization. Or, an arbitrary "sufficiently high" lower bound on the conductivity coefficient k, i.e. in a manner analogous with structural reinforcement problems, can be defined to make sure that low density elements have sufficient conductivity to hopefully prevent the oscillations.

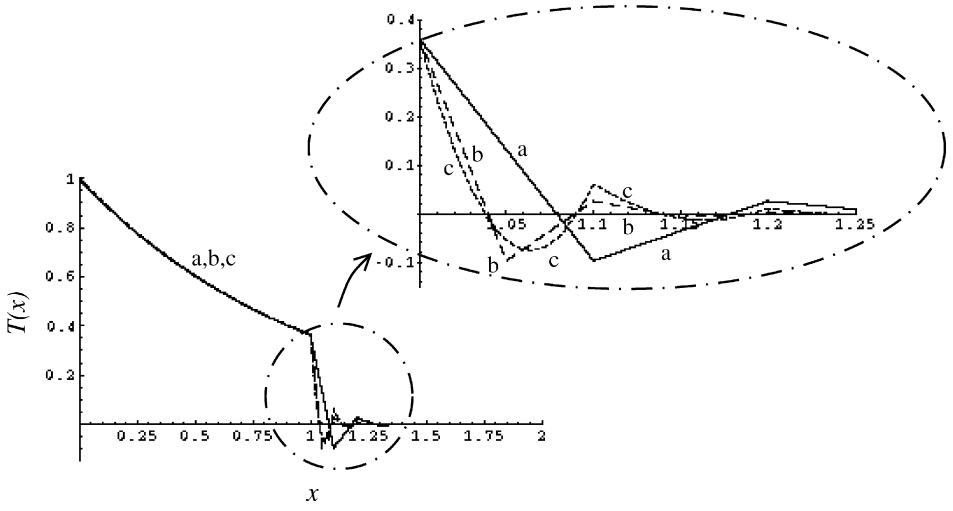

Fig. 8. (P1) Finite element excess temperature response $T(x)$ for vanishing Ω_2 with one-dimensional, (a) 20 two-noded, (b) 40 two-noded (h-refinement), and (c) 20 3-noded (p-refinement) elements.

Alternatively, because the temperature response should be bounded from below by θ^*, the author has numerically fixed any nodal temperature $\theta < \theta^*$ to $\theta = \theta^*$ iteratively until all nodal temperatures satisfy $\theta \geqslant \theta^*$ (in a similar manner as the methodology to remove rigid body modes described in [39,40]) with some success. Since the oscillations arise because the continuous finite element interpolation cannot capture the discontinuous temperature response over a finite element, cf. Fig. 6b and Fig. 8 at the Ω_1–Ω_2 interface, discontinuous Galerkin (DG) methods are a more appropriate numerical method for this problem, but the computational overhead of these methods seems problematic for large-scale topology optimization.

Key insights into resolving the numerical instabilities are that (1) the oscillations are due to convection-dominated diffusion and that (2) the convection boundary conditions are numerically enforced in a manner analogous to a penalty method. For the first insight, since the conduction terms are density dependent while the volumetric convection terms are fixed, the analysis becomes dominated by the convection terms in those elements with low density. Moreover, although the positive contributions of the off-diagonal terms of the consistent convection matrix, e.g. in Eq. (39), do not pose an inherent numerical problem, the magnitude of their presence in relation to the magnitude of the diagonal terms gives rise to the numerical oscillations. For the second insight, rather than reordering the governing equations, we recognize that a common approach to applying boundary conditions is to enforce the boundary conditions by adding an equation of the form

$$\alpha\theta = \alpha\theta^* \tag{41}$$

where a "sufficiently large" penalty parameter α enforces the desired boundary condition $\theta = \theta^*$. The role of the physical convection coefficient h in Eq. (7) mimics the effect of enforcing the boundary condition numerically by penalty parameter α in Eq. (41). Therefore, we should not be surprised that the brute enforcement of *boundary* conditions on the interior of the domain while maintaining the FEA continuity conditions can cause potential numerical problems. We can enforce the boundary conditions strongly at the finite element nodes, but we can only enforce the boundary conditions in a weighted-average sense in the interior of any finite element.

As an aside, the second insight leads naturally to the alternative topology optimization by penalty (TOP) method [41]. In this formulation, existing topology optimization formulations are reinterpreted, e.g. for fluid mechanics, and alternatively formulated, e.g. in the design of supports, and the methodology opens the possibility of solving new problems, e.g. for mechanism design.

Based on our insights, we resolve the numerical instabilities by ensuring that the convection term contributions are so-called lumped matrices. This can be accomplished readily in two ways. Firstly, we can evaluate the convection matrices directly in lumped form, e.g. by

$$\mathbf{K}^h = \frac{h}{2}\begin{bmatrix} 1 & 0 \\ 0 & 1 \end{bmatrix} \tag{42}$$

for the one-dimensional heat transfer problem P1. The topic of matrix diagonalization or lumping for FEA is expounded upon in appendix 8 of Ref. [42]. Secondly, we can ensure that the convection matrix becomes diagonal as the domain of interest vanishes, i.e. by modifying the consistent convection matrix of P1 to

$$\mathbf{K}^h = \frac{\bar{h}}{6}\begin{bmatrix} 2 & d \\ d & 2 \end{bmatrix} \tag{43}$$

where the nominal $\bar{h}$ is fixed and variable $\underline{d} \leqslant d \leqslant 1$ indicates the relative absence, e.g. $d = \underline{d} = 10^{-6}$, or presence, i.e. $d = 1$, of the domain. Note that we want the off-diagonal terms of Eq. (43) to equal zero when $d = 0$ and equal one when $d = 1$. We have chosen a linear interpolation here, but for intermediate d values, it may be preferable in terms of numerical stability that the off-diagonal terms be interpolated between zero and one by a nonlinear interpolation scheme, e.g. by d^p for penalty parameter $p > 1$, in the topology optimization.

We return to the FEA solution of problem P1 with lumped matrix in the form of Eq. (42) and set $k_2 = 10^{-6}\,\frac{\mathrm{W}}{\mathrm{m}\,^\circ\mathrm{C}}$, $h_{12} = 1\,\frac{\mathrm{W}}{\mathrm{m}^2\,^\circ\mathrm{C}}$, and $h_{2e} = 0\,\frac{\mathrm{W}}{\mathrm{m}^2\,^\circ\mathrm{C}}$, and $h_2 = h_1 = 1\,\frac{\mathrm{W}}{\mathrm{m}^2\,^\circ\mathrm{C}}$, and Fig. 9 shows the FEA response. Note that there are no oscillations in the temperature response and that the FEA solution approaches the analytical solution

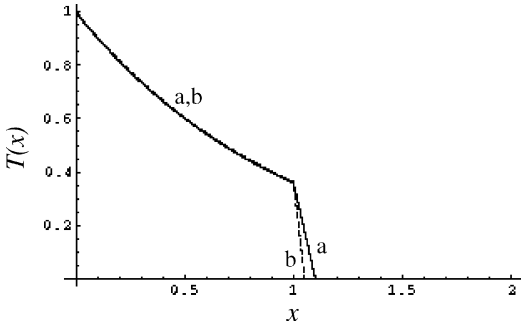

Fig. 9. (P1) Finite element excess temperature response $T(x)$ for vanishing Ω_2 with one-dimensional, (a) 20 two-noded and (b) 40 two-noded (h-refinement) elements.

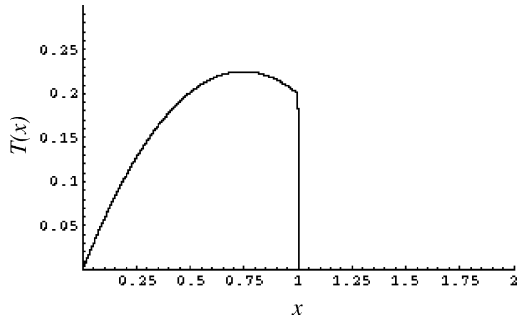

Fig. 10. (P2) Analytical excess temperature response $T(x)$ for absent/vanishing Ω_2.

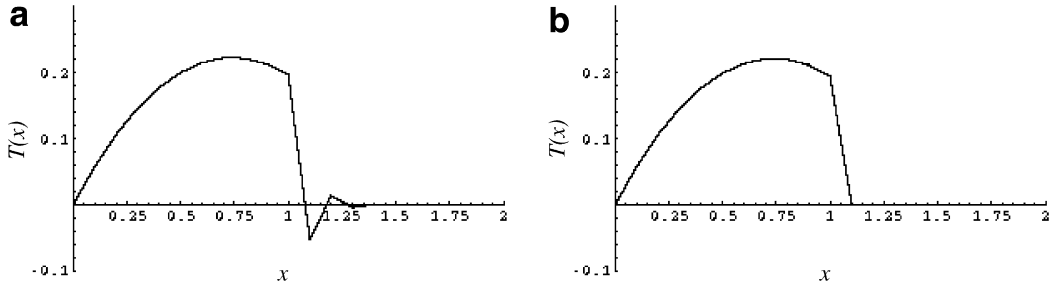

Fig. 11. (P2) Finite element excess temperature response $T(x)$ for vanishing Ω_2 with one-dimensional, 20 two-noded elements and (a) consistent or (b) lumped convection matrices.

of Fig. 6b with refinement, e.g. by *h*-refinement as shown in Fig. 9b.

Next, we briefly investigate the temperature response of problem P2 of Fig. 5b as domain Ω_2 vanishes. For Ω_1, we set $L_1 = 1$ m, $k_1 = 1\ \frac{\mathrm{W}}{\mathrm{m}\ ^\circ\mathrm{C}}$, $h_1 = 1\ \frac{\mathrm{W}}{\mathrm{m}^2\ ^\circ\mathrm{C}}$, and $Q_1 = 1$ W, and for vanishing Ω_2, we set $L_2 - L_1 = 1$ m, $k_2 = 10^{-6}\ \frac{\mathrm{W}}{\mathrm{m}\ ^\circ\mathrm{C}}$, $h_2 = 1\ \frac{\mathrm{W}}{\mathrm{m}^2\ ^\circ\mathrm{C}}$, $h_{12} = 1\ \frac{\mathrm{W}}{\mathrm{m}^2\ ^\circ\mathrm{C}}$, $h_{2e} = 0\ \frac{\mathrm{W}}{\mathrm{m}^2\ ^\circ\mathrm{C}}$, and $Q_2 = 10^{-6}$ W. For P2, we prescribe the base temperature $\theta_b^* = 0\ ^\circ\mathrm{C}$ and the ambient fluid temperature $\theta^* = 0\ ^\circ\mathrm{C}$ again. The corresponding temperature response is depicted in Fig. 10. Note again that h_{12} is sufficiently large to drive the temperature response to the ambient fluid temperature θ^* at the Ω_1–Ω_2 interface. As Fig. 11a demonstrates, nonphysical oscillations appear in FEA solution using consistent convection matrix of Eq. (40), so the lumped convection matrix of Eq. (42) is used instead, and the corresponding FEA solution is shown in Fig. 11b. Note that the oscillations are suppressed when a lumped convection matrix is implemented.

Fig. 12 shows the effect of varying Q_2 on the temperature response which indicates that we desire $Q_2 \to 0$ as Ω_2 vanishes. Therefore, as a cautionary note, in cases where Q_2 is held constant, e.g. when the design domain rests on top of a conductive substrate, a lower bound on k_2 should be "sufficiently large" to ensure that the temperature response remains realistic. Furthermore, conditions under which the domain interior experiences excessive heat flux due to regions of low density elements, particularly at intermediate optimization iterations, can lead to divergence of the nonlinear FEA solution by the Newton–Raphson method. Although we do not experience divergence problems in the examples presented below, they can be readily resolved by the techniques employed for the gross mesh distortion of regions of low density elements in structural topology optimization problems, e.g. see the discussion in [39].

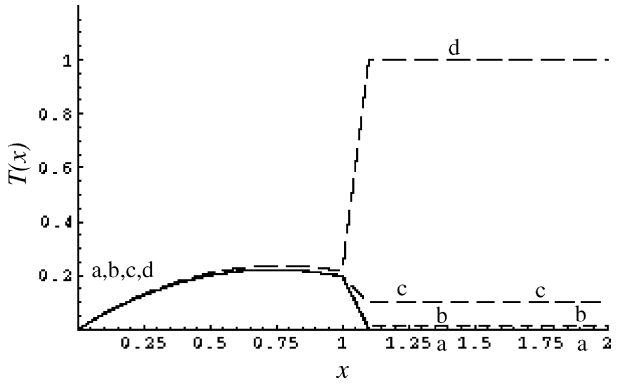

Fig. 12. (P2) Effect of varying (a) $Q_2 = 10^{-6}$, (b) 10^{-2}, (c) 10^{-1}, and (d) 1 W on the excess temperature response $T(x)$.

Until now, we have not discussed how to implement side convection, i.e. h_{12} and h_{2e} type terms, into the FEA for topology optimization. This is a nontrivial issue because the optimization progress will be heavily influenced by the particular density-based side convection formulation. For the present problems, we do not incorporate side convection, which will also cause numerical instabilities that can be resolved by the methodology described here, so that we can more directly examine the source of the oscillatory behavior. However, we advocate the following approach for planar problems which is described more thoroughly in [32]. In summary, the side convection terms are weighted by a density-difference-based interpolation scheme, and half of the total contribution is associated which each of the two elements connected along the same edge so that the total convection contribution is easily applied on summing over each element in the usual finite element procedure. For example, for elements i and j connected by a common interface, i.e. edge, with corresponding densities d_i and d_j, the nominal side convection coefficient $\bar{h}$ can be interpolated by:

$$h_i = \frac{1}{2} g(d_i - d_j)\bar{h} \quad \text{and} \quad h_j = \frac{1}{2} g(d_j - d_i)\bar{h} \quad \text{where e.g. } g(\rho) \approx |\rho| \tag{44}$$

where h_i and h_j are the side convection coefficients used in the element computations. In density-design-variable-based topology optimization, the solid–void interface is diffuse at intermediate optimization iterations, and therefore, tracking it is problematic from an implementation point of view. By distributing half the contribution to both sides of the interface and accounting for sign changes via function g due to the density differences and the opposing directions of the outward-facing normals, we do not need to track where the interface is nor apply terms on only one side of the interface. This approach can be adapted

for boundary conditions in the domain interior of other mechanics problems, e.g. electrostatics and pressure loads.

Before concluding, we note that we did not explicitly account for fluid motion in the discussion of Section 2. To do so, we add the convective term to the right-hand-side of Eq. (3) as

$$-\mathrm{div}\,\mathbf{q}(\mathbf{x}) + s(\mathbf{x}) = \rho c_\mathrm{p}\mathbf{v}(\mathbf{x})\cdot\nabla\theta(\mathbf{x}) \tag{45}$$

where ρ is the fluid density, c_p is the specific heat at constant pressure p, and $\mathbf{v}$ is the fluid velocity vector. It should be noted that extensive research in the past half century has been devoted to resolving the nonphysical oscillatory behavior in convection-dominated heat and fluid flow that appears in the FEA solution. For example, refer to chapter 12 of [43] and the references contained therein for an introduction. The jumps in material properties that physically occur in stationary and moving interface problems such as for solidification simulation are analogous to the jumps in material properties that occur topology optimization. Stabilized solution strategies have been studied extensively for these problems, e.g. see [44,45]. Our purpose here is to merely point out that the stability issue will be encountered as topology optimization is expanded to design problems with more complex mechanics. In [46], we more thoroughly examine the oscillatory behavior and its ramifications on the topology optimization for fluid mechanics problems.

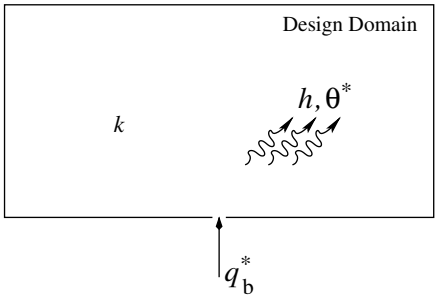

Fig. 13. (P3) Design domain for micro-cooling fins.

5. Examples

In problem P3, we design micro-cooling fins for the design domain depicted in Fig. 13. The $40\times 20\ \mu\mathrm{m}^2$ domain with uniform 1 μm thickness is discretized by 3200 uniform 4-node quadrilateral element mesh. A heat flux $q_\mathrm{b}^* = 1\,\frac{p\mathrm{W}}{\mu\mathrm{m}^2}$ is prescribed at the mid-span of the lower edge. The conductivity of the constituent material is $k = 1\,\frac{p\mathrm{W}}{\mu\mathrm{m}\ ^\circ\mathrm{C}}$. We assume that convection occurs predominantly from the top surface only with convection coefficient $h = 10^{-3}\,\frac{p\mathrm{W}}{\mu\mathrm{m}^2\ ^\circ\mathrm{C}}$ and ambient fluid temperature $\theta^* = 0\ ^\circ\mathrm{C}$. The design objective is to optimally distribute material so that the temperature at the applied heat flux is minimized, i.e. minimize $\Theta_0 = \theta_\mathrm{b}$, subject to a material resource constraint, i.e. the upper bound on the total volume $\overline{v}$ is set to 30% of the maximal volume. The density design variables are initially set to $d_j = 0.2$, and their lower and upper bounds are set to $\underline{d}_j = 10^{-9}$ and $\bar{d}_j = 1$, respectively. For the SINH method, the filter length r is set to 1 μm, and the penalty parameter p is fixed at $p = 3$.

Fig. 14 depicts the optimization history of the topology design using consistent convection matrices. The optimized temperature is $\theta_\mathrm{b} = 3.37\ ^\circ\mathrm{C}$ at iteration 680, and the temperature ranges from 0.19 to 3.37 °C in the design domain as shown in Fig. 15h. Fig. 15b–g indicate that the temperature drops below θ^* in the black regions due to unphysical oscillations in the temperature response. It is fortuitous that the optimization algorithm does not appear to take advantage of the numerical oscillations in this problem, but in general, we cannot guarantee that the optimization history will not be unduly affected.

To resolve the numerical instabilities, we generate optimized topologies using explicitly lumped convection matrices, i.e. analogous to Eq. (42), and density-based lumped convection matrices, i.e. analogous to Eq. (43). Figs. 16 and 18 depict the respective optimization history of the topology design using lumped convection matrices. The optimized temperatures are $\theta_\mathrm{b} = 3.37\ ^\circ\mathrm{C}$ at iteration 528 and $\theta_\mathrm{b} = 3.41\ ^\circ\mathrm{C}$ at iteration 767 respectively, and the temperature ranges from $9.8\times 10^{-2} - 3.37\ ^\circ\mathrm{C}$ to $5.5\times 10^{-13} - 3.41\ ^\circ\mathrm{C}$ in the design domains as shown in Figs. 17 and

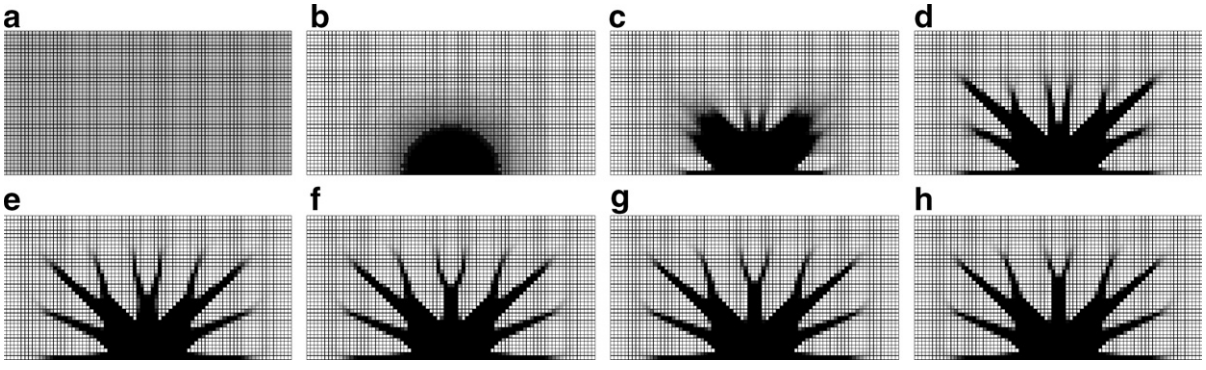

Fig. 14. (P3) Topology optimization history plots of first density measures $\boldsymbol{\eta}_1$ at iteration (a) 0, (b) 24, (c) 72, (d) 120, (e) 192, (f) 264, (g) 336, and (h) 680 using consistent convection matrices.

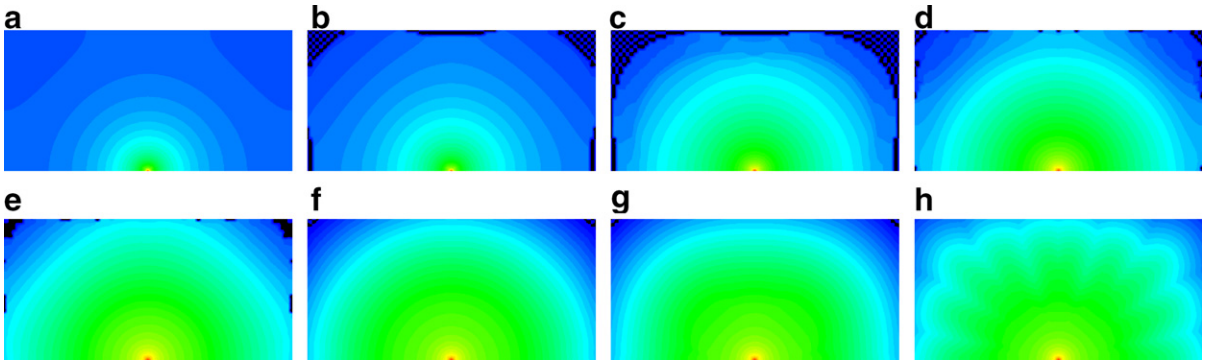

Fig. 15. (P3) Topology optimization history plots of temperature response at iteration (a) 0, (b) 3, (c) 6, (d) 9, (e) 15, (f) 36, (g) 63, and (h) 680 using consistent convection matrices.

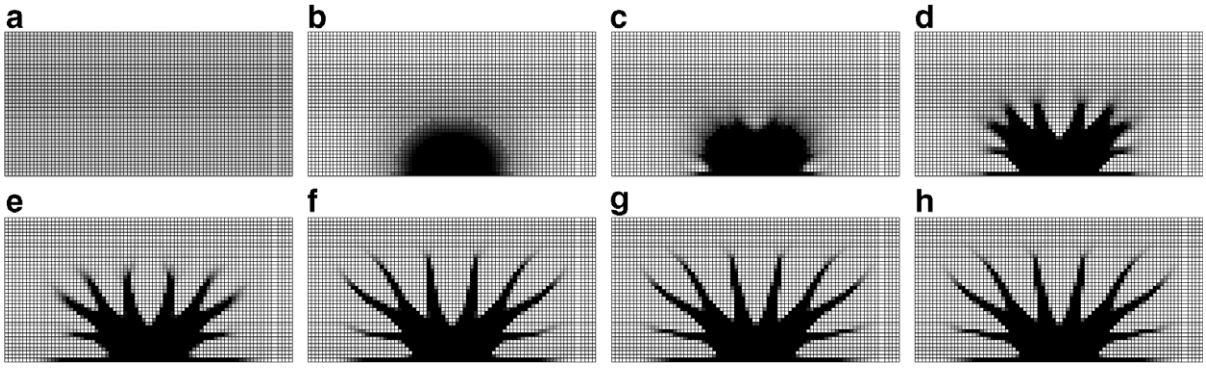

Fig. 16. (P3) Topology optimization history plots of first density measures η_1 at iteration (a) 0, (b) 24, (c) 48, (d) 72, (e) 96, (f) 192, (g) 384, and (h) 528 using explicitly lumped convection matrices.

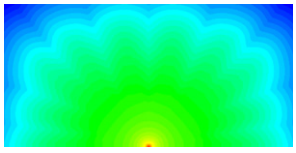

Fig. 17. (P3) Topology optimization plot of temperature response at iteration 528 using explicitly lumped convection matrices.

19 respectively. No oscillation appears in the temperature response at any intermediate optimization iteration using the lumped convection matrices. Note also that the density-based lumped convection matrix formulation enforces the ambient fluid temperature more aggressively than the other formulations. Furthermore, we generate different optimized topologies on comparison of Figs. 14h, 16h, and 18h. This can be attributed to the different numerical schemes to model the physical convection and to the numerous local minima in the design space that is searched by a gradient-based nonlinear programming algorithm.

In problem P4, we design another micro-cooling fin for the design domain depicted in Fig. 20. The $40 \times 20\ \mu m^2$

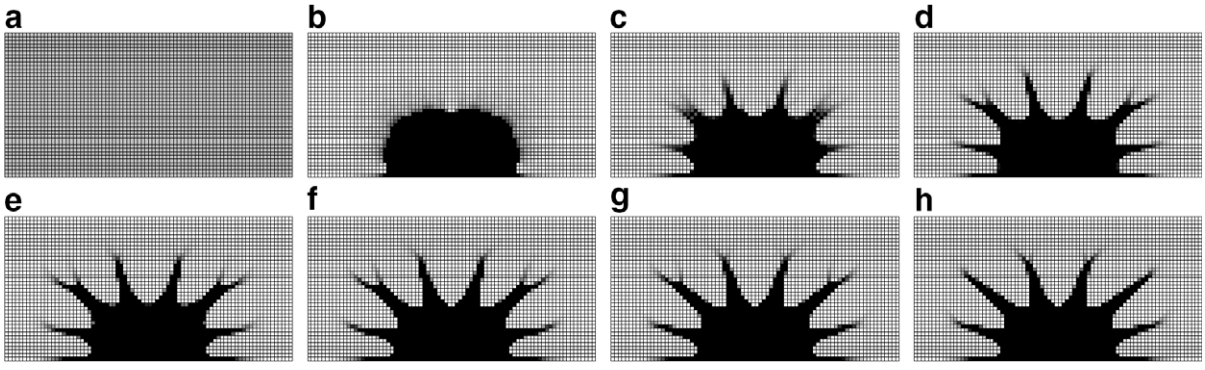

Fig. 18. (P3) Topology optimization history plots of first density measures η_1 at iteration (a) 0, (b) 96, (c) 124, (d) 148, (e) 172, (f) 224, (g) 336, and (h) 767 using density-based lumped convection matrices.

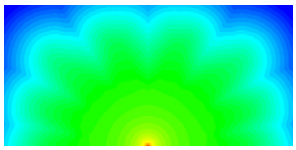

Fig. 19. (P3) Topology optimization plot of temperature response at iteration 767 using density-based lumped convection matrices.

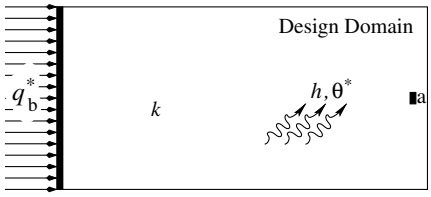

Fig. 20. (P4) Design domain for micro-cooling fin.

domain with uniform 1 μm thickness is discretized by 3200 uniform 4-node quadrilateral element mesh. A heat flux $q^*_b = 1\frac{pW}{\mu m^2}$ is prescribed along the left domain edge. The conductivity of the nonlinear constituent material is $k = 1 + 0.1\theta\frac{pW}{\mu m\,^\circ C}$. We assume that convection occurs predominantly from the top surface only with convection coefficient $h = 10^{-1}\frac{pW}{\mu m^2\,^\circ C}$ and ambient fluid temperature $\theta^* = 0\,^\circ C$. The design objective is to optimally distribute material so that the temperature at tip point 'a' (39 mm, 10 mm) is maximized, i.e. minimize $\Theta_0 = -\theta_a$, subject to a material resource constraint, i.e. the upper bound on the total volume $\bar{v}$ is set to 30% of the maximal volume. The density at the left edge and about point 'a' are fixed as solid, i.e. $d_j = 1$, and the rest of the density design variables are initially set to $d_j = 0.2$, and their lower and upper bounds are set to $\underline{d}_j = 10^{-9}$ and $\overline{d}_j = 1$, respectively. For the SINH method, the filter length r is set to 1 μm, and the penalty parameter p is fixed at $p = 3$.

Fig. 21 depicts the optimization history of the topology design using consistent convection matrices. The optimized temperature is $\theta_a = 5.27 \times 10^{-5}\,^\circ C$ at iteration 152, and the temperature ranges from -3.81 to $10.44\,^\circ C$ in the design domain as shown in Fig. 22h. Fig. 22b–g indicates that the temperature drops below θ^* in the black regions due to unphysical oscillations in the temperature response.

To resolve the numerical instabilities, we generate optimized topologies using explicitly lumped convection matrices, i.e. analogous to Eq. (42). Fig. 23 depicts the optimization history of the topology design. The optimized temperature is $\theta_a = 4.01 \times 10^{-5}\,^\circ C$ at iteration 159, and the temperature ranges from 0 to $9.85\,^\circ C$ in the design domains as shown in Fig. 24.

Finally in problem P5, we solve problem P4 again with higher nonlinear conductivity $k = 100 + 10\theta\frac{pW}{\mu m\,^\circ C}$. Fig. 25

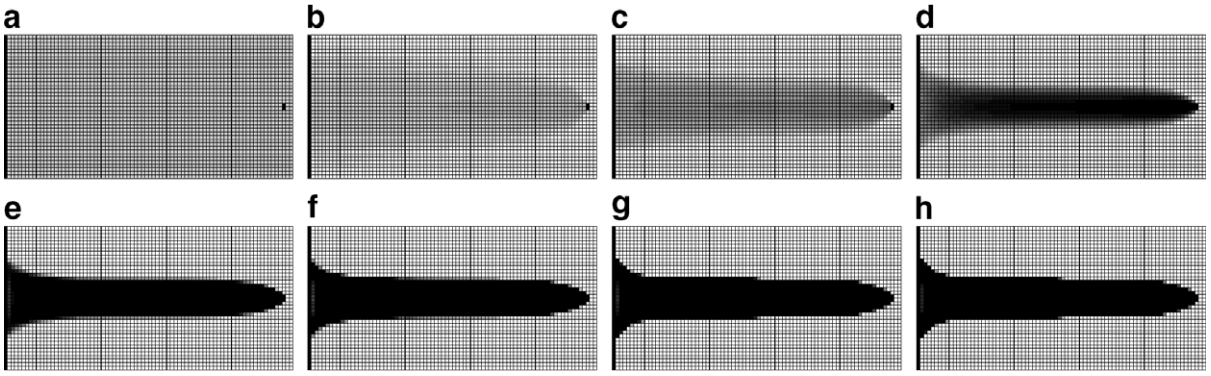

Fig. 21. (P4) Topology optimization history plots of first density measures η_1 at iteration (a) 0, (b) 5, (c) 10, (d) 20, (e) 30, (f) 50, (g) 100, and (h) 152 using consistent convection matrices.

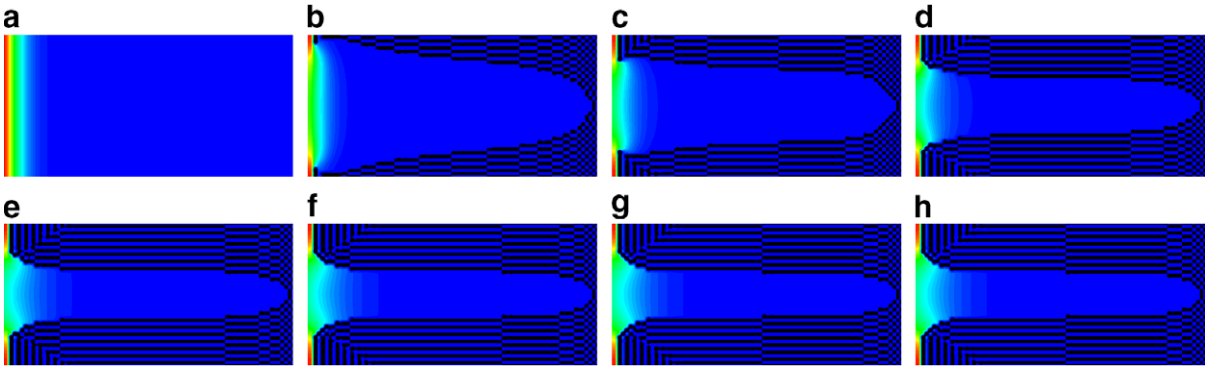

Fig. 22. (P4) Topology optimization history plots of temperature response at iteration (a) 0, (b) 5, (c) 10, (d) 20, (e) 30, (f) 50, (g) 100, and (h) 152 using consistent convection matrices.

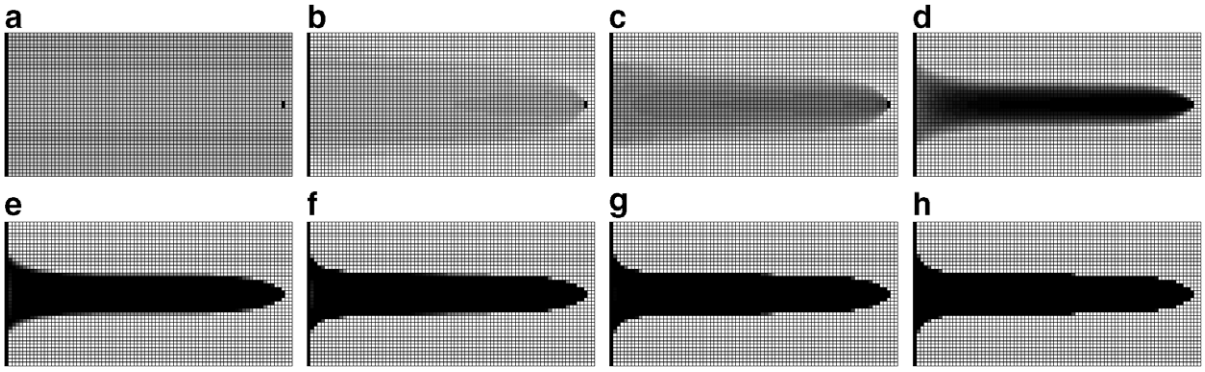

Fig. 23. (P4) Topology optimization history plots of first density measures η_1 at iteration (a) 0, (b) 5, (c) 10, (d) 20, (e) 30, (f) 50, (g) 100, and (h) 159 using explicitly lumped convection matrices.

Fig. 24. (P4) Topology optimization plot of temperature response at iteration 159 using explicitly lumped convection matrices.

depicts the optimization history of the topology design using consistent convection matrices. The optimized temperature is $\theta_a = 0.66$ °C at iteration 143, and the temperature ranges from −0.86 to 1.29 °C in the design domain as shown in Fig. 26h. Fig. 26b–g indicate that the temperature drops below θ^* in the black regions due to unphysical oscillations in the temperature response.

Fig. 27 depicts the optimization history of the topology design using explicitly lumped convection matrices, i.e.

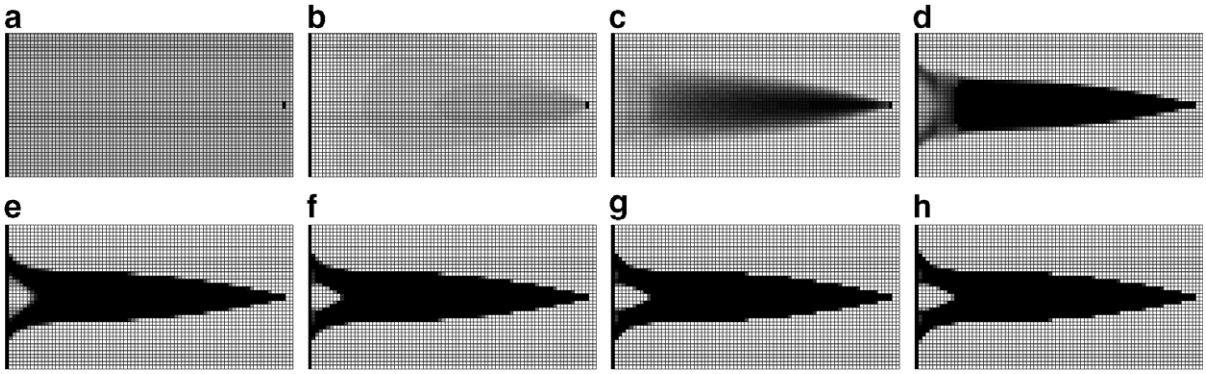

Fig. 25. (P5) Topology optimization history plots of first density measures η_1 at iteration (a) 0, (b) 15, (c) 30, (d) 40, (e) 50, (f) 60, (g) 80, and (h) 143 using consistent convection matrices.

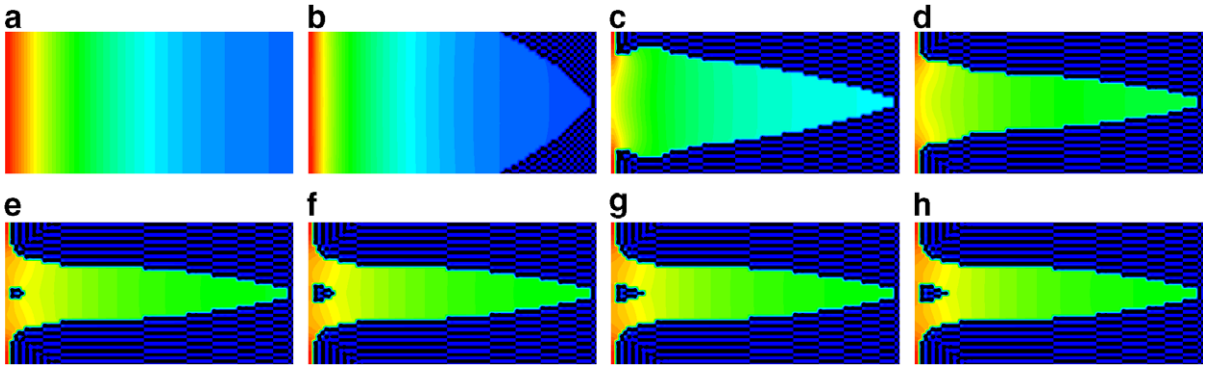

Fig. 26. (P5) Topology optimization history plots of temperature response at iteration (a) 0, (b) 15, (c) 30, (d) 40, (e) 50, (f) 60, (g) 80, and (h) 143 using consistent convection matrices.

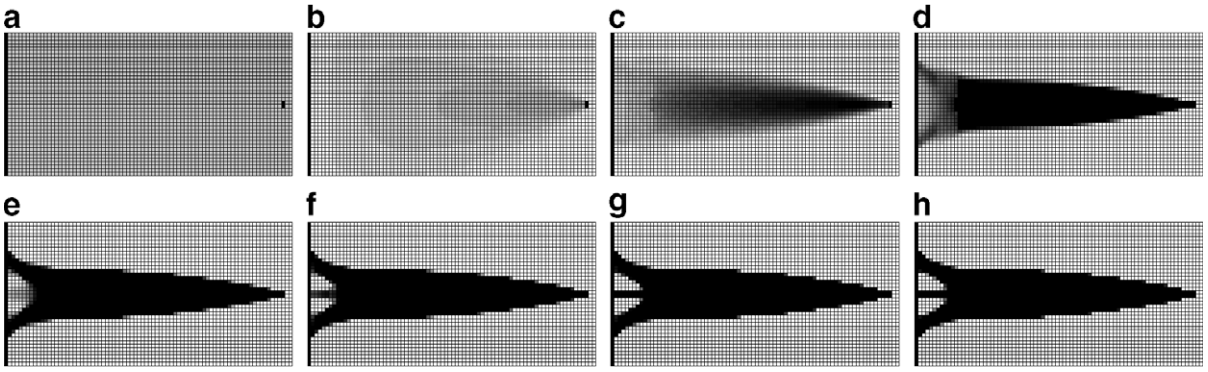

Fig. 27. (P5) Topology optimization history plots of first density measures η_1 at iteration (a) 0, (b) 15, (c) 30, (d) 40, (e) 50, (f) 60, (g) 80, and (h) 108 using explicitly lumped convection matrices.

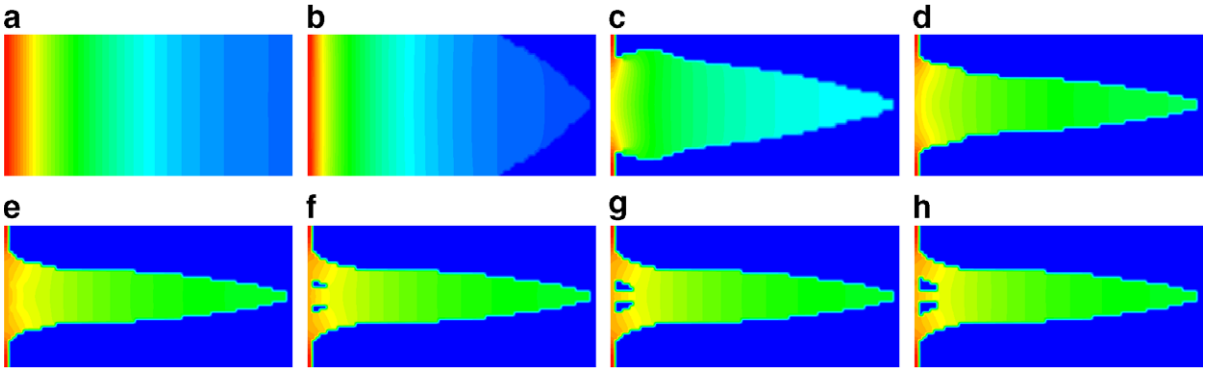

Fig. 28. (P5) Topology optimization history plots of temperature response at iteration (a) 0, (b) 15, (c) 30, (d) 40, (e) 50, (f) 60, (g) 80, and (h) 108 using explicitly lumped convection matrices.

analogous to Eq. (42). The optimized temperature is $\theta_a = 0.62\,^{\circ}\mathrm{C}$ at iteration 108, and the temperature ranges from 0 to 1.26 °C in the design domains as shown in Fig. 28. Note that the oscillations that develop in the region of low density elements at the base of the fin, e.g. in Fig. 26e, lead to a different design at the base.

6. Conclusion

We have demonstrated that numerical problems in the FEA can develop when convection is applied in a consistent manner. Most notably, nonphysical oscillations in the regions of low density, and consequently low conductivity, elements in the FEA solution indicate that numerical problems exist. Consequently, the poor modeling of convection can adversely influence the design space search of the optimization algorithm, e.g. particularly for multiphysics design problems where other physics are coupled to the thermal analysis. To resolve this issue, we implement lumped convection, and the examples demonstrate that the spurious oscillations are removed from the FEA.

Acknowledgement

The author is grateful for the funding provided by the Arnold and Mabel Beckman Foundation.

References

[1] Q. Li, G.P. Steven, Y.M. Xie, O.M. Querin, Evolutionary topology optimization for temperature reduction of conducting fields, Int. J. Heat Mass Transfer 47 (2004) 5071–5083.
[2] T. Borrvall, A. Klarbring, J. Petersson, B. Torstenfelt, Topology optimization in fluid mechanics, in: Proceedings of the 5th World Congress on Computational Mechanics, Vienna, Austria, July 2002.
[3] M.P. Bendsøe, O. Sigmund, Topology Optimization: Theory, Methods and Applications, Springer-Verlag, New York, 2003.
[4] H.C. Rodrigues, P. Fernandes, Topology optimal design of thermoelastic structures using a homogenization method, Control Cybern. 23 (3) (1994) 553–563.
[5] H.C. Rodrigues, P. Fernandes, A material based model for topology optimization of thermoelastic structures, Int. J. Numer. Meth. Eng. 38 (1995) 1951–1965.
[6] C. Jog, Distributed-parameter optimization and topology design for non-linear thermoelasticity, Comput. Meth. Appl. Mech. Eng. 132 (1996) 117–134.
[7] Q. Li, G.P. Steven, Y.M. Xie, Displacement minimization of thermoelastic structures by evolutionary thickness design, Comput. Meth. Appl. Mech. Eng. 179 (1999) 361–378.
[8] Q. Li, G.P. Steven, O.M. Querin, Y.M. Xie, Shape and topology design for heat conduction by evolutionary structural optimization, Int. J. Heat Mass Transfer 42 (1999) 3361–3371.
[9] Q. Li, G.P. Steven, O.M. Querin, Y.M. Xie, Structural topology design with multiple thermal criteria, Eng. Comput. 17 (6) (2000) 715–734.
[10] Q. Li, G.P. Steven, Y.M. Xie, Thermoelastic topology optimization for problems with varying temperature fields, J. Therm. Stress. 24 (2001) 347–366.

[11] G.P. Steven, Q. Li, Y.M. Xie, Evolutionary topology and shape design for general physical field problems, Comput. Mech. 26 (2000) 129–139.
[12] E.C.N. Silva, J.S.O. Fonseca, N. Kikuchi, Optimal design of periodic piezocomposities, Comput. Meth. Appl. Mech. Eng. 159 (1998) 49–77.
[13] E.C.N. Silva, N. Kikuchi, Design of piezoelectric transducers using topology optimization, Smart Mater. Struct. 8 (1999) 350–364.
[14] Y. Li, K. Saitou, N. Kikuchi, Topology optimization of thermally actuated compliant mechanisms considering time-transient effect, Finite Element. Anal. Design 40 (2004) 1317–1331.
[15] J.-K. Byun, I.-H. Park, S.-Y. Hahn, Topology optimization of electrostatic actuator using design sensitivity, IEEE Trans. Magnet. 38 (2) (2002) 1053–1056.
[16] R.H.W. Hoppe, S.I. Petrova, V. Schultz, Primal-dual newton-type interior-point method for topology optimization, J. Optim. Theory Appl. 114 (3) (2002) 545–571.
[17] S. Wang, S. Park, J. Kang, Multi-domain topology optimization of electromagnetic systems, Int. J. Comput. Math. Electric. Electron. Eng. 23 (4) (2004) 1036–1044.
[18] O. Sigmund, S. Torquato. Design of materials with extreme thermal expansion using a three-phase topology optimization method, J. Mech. Phys. Solids 45 (6) (1997) 1037–1067.
[19] O. Sigmund, S. Torquato, I.A. Aksay, On the design of 1–3 piezocomposites using topology optimization, J. Mater. Res. 13 (4) (1997) 1038–1048.
[20] O. Sigmund, S. Torquato, Design of smart composite materials using topology optimization, Smart Mater. Struct. 8 (1997) 365–379.
[21] J. Jonsmann, O. Sigmund, S. Bouwstra, Compliant thermal micro-actuators, Sensors Actuators A 76 (1999) 463–469.
[22] O. Sigmund, Design of multiphysics actuators using topology optimization – Part I: one-material structures, Comput. Meth. Appl. Mech. Eng. 190 (2001) 6577–6604.
[23] O. Sigmund, Design of multiphysics actuators using topology optimization - Part II: two-material structures, Comput. Meth. Appl. Mech. Eng. 190 (2001) 6605–6627.
[24] L. Yin, G.K. Ananthasuresh, A novel topology design scheme for the multi-physics problems of electro-thermally actuated compliant micromechanisms, Sensors Actuators A 97–98 (2002) 599–609.
[25] G.H. Yoon, Y.Y. Kim, Topological optimization for multiphysics problems using the element connectivity parameterization method, in: Proceedings of the 10th AIAA/ISSMO Multidisciplinary Analysis and Optimization Conference, Albany, New York, August 30–September 1, 2004.
[26] M. Allen, M. Raulli, K. Maute, D.M. Frangopol, Reliability-based analysis and design optimization of electrostatically actuated mems, Comput. Struct. 82 (2004) 1007–1020.
[27] M. Raulli, K. Maute, Topology optimization of electrostatic MEMS, in: Proceedings of the 10th AIAA/ISSMO Multidisciplinary Analysis and Optimization Conference, Albany, New York, August 30–September 1 2004.
[28] T.E. Bruns, O. Sigmund, Toward the topology design of mechanisms that exhibit snap-through behavior, Comput. Meth. Appl. Mech. Eng. 193 (2004) 3973–4000.
[29] Y. Ha, M.-G. Kim, S. Cho, Topology optimization of nonlinear heat conduction problems using adjoint design sensitivity analysis method, in: Proceedings of the 10th AIAA/ISSMO Multidisciplinary Analysis and Optimization Conference, Albany, New York, August 30–September 1, 2004.
[30] H. Moon, C. Kim, S. Wang, Reliability-based topology optimization of thermal systems considering convection heat transfer, in: Proceedings of the 10th AIAA/ISSMO Multidisciplinary Analysis and Optimization Conference, Albany, New York, August 30–September 1, 2004.
[31] P.M. Gresho, R.L. Lee, Don't suppress the wiggles – they're telling you something, in: T.J.R. Hughes (Ed.), Finite Element Methods for Convection Dominated Flows, Proceedings of the ASME, vol. AMD 34, New York, December 2–7, 1979.
[32] T.E. Bruns, Topology optimization of MEM devices, in preparation.
[33] K.-J. Bathe, Finite Element Procedures, Prentice-Hall, Upper Saddle River, New Jersey, 1996.
[34] M.P. Bendsøe, Optimal shape design as a material distribution problem, Struct. Optim. 1 (1989) 193–202.
[35] M. Zhou, G.I.N. Rozvany, The COC algorithm, Part II: topological, geometrical and generalized shape optimization, Comput. Meth. Appl. Mech. Eng. 89 (1991) 309–336.
[36] T.E. Bruns, A reevaluation of the SIMP method with filtering and an alternative formulation for solid-void topology optimization, Struct. Multidiscip. Optim. 30 (6) (2005) 428–436.
[37] E.J. Haug, K.K. Choi, V. Komkov, Design Sensitivity Analysis of Structural Systems, Academic Press, Inc., New York, 1986.
[38] K. Svanberg, Method of moving asymptotes – a new method for structural optimization, Int. J. Numer. Meth. Eng. 24 (2) (1987) 359–373.
[39] T.E. Bruns, D.A. Tortorelli, An element removal and reintroduction strategy for the topology optimization of structures and compliant mechanisms, Int. J. Numer. Meth. Eng. 57 (10) (2003) 1413–1430.
[40] T.E. Bruns, Zero density lower bounds in topology optimization, Comput. Meth. Appl. Mech. Eng. 196 (2006) 566–578.
[41] T.E. Bruns, Topology optimization by penalty (TOP) method, in: Proceedings of the 6th World Congress of Structural and Multidisciplinary Optimization, Rio de Janeiro, Brazil, May 30–June 3, 2005.
[42] O.C. Zienkiewicz, R.L. Taylor, The Finite Element Method, Basic Formulations and Linear Problems, fourth ed., vol. 1, McGraw-Hill, New York, 1989.
[43] O.C. Zienkiewicz, R.L. Taylor, The Finite Element Method, Solid and Fluid Mechanics, Dynamics, and Non-linearity, fourth ed., vol. 2, McGraw-Hill, New York, 1991.
[44] H.S. Udaykumar, R. Mittal, W. Shyy, Computation of solid-liquid phase fronts in the sharp interface limits on fixed grids, J. Comput. Phys. 153 (1999) 535–574.
[45] E. Bänsch, A. Schmidt, Simulation of dendritic crystal growth with thermal convection, Interfaces Free Bound. 2 (2000) 95–115.
[46] T.E. Bruns, Topology optimization for fluid mechanics, in preparation.